Constrained Reconstruction of Sparse Cardiac MR DTI Data

Ganesh Adluru[1,3], Edward Hsu[2], and Edward V.R. DiBella[2,3]

[1] Electrical and Computer Engineering department, 50 S. Central Campus Dr., MEB, University of Utah, Salt Lake City, UT, USA
gadluru@sci.utah.edu
[2] Department of Bioengineering, 50 S Central Campus Dr., University of Utah, Salt Lake City, UT, USA
edward.hsu@utah.edu
[3] UCAIR, Department of Radiology, 729 Arapeen Dr., University of Utah, Salt Lake City, UT, USA
ed@ucair.med.utah.edu

Abstract. Magnetic resonance diffusion tensor imaging (DTI) has emerged as a convenient and reliable alternative to conventional histology for characterizing the fiber structure of the myocardium. The acquisition of full data for different diffusion directions for a large number of slices often takes a long time and results in trade-offs in the number of slices and signal to noise ratios. We propose a constrained reconstruction technique based on a regularization framework to jointly reconstruct sparse sets of cardiac DTI data. Constraints on spatial variation and directional variation were used in the reconstruction. The method was tested on sparse data undersampled in both rectilinear and (simulated) radial fashions and compared to reconstructions from full data. The method provided reasonable reconstructions with half of the data for rectilinear undersampling and similar quality images with a quarter of the data if radial undersampling was used.

1 Introduction

The fiber structure of the myocardium plays a key role in determining the anisotropic mechanical and electrophysiological properties of the tissue. DTI has emerged as a convenient and reliable alternative to conventional histology for characterizing the fiber structure of the myocardium [1]. A limitation of current cardiac DTI is the long acquisition time, which often results in tradeoffs in the number of slices and signal to noise ratios. Methods [2, 3] have been proposed to reduce the acquisition time by acquiring sparse data in k-space for each orientation and reconstructing each image direction separately. The methods achieved accelerations up to a factor of two (R=2, using half of the data), but often require acquiring additional reference data. Also these methods do not exploit the correlations in the dimension of diffusion direction. Typically 6-12 or more diffusion directions are measured separately. We recently proposed a spatio-temporal constrained reconstruction framework to reconstruct sparse dynamic contrast enhanced MRI data. The method is based on regularizing the

F.B. Sachse and G. Seemann (Eds.): FIMH 2007, LNCS 4466, pp. 91–99, 2007.

data in both space and time dimensions and is applied to reconstructing dynamic cardiac perfusion images [4] from sparse data. A similar framework is proposed here to apply instead to space and diffusion dimensions to jointly reconstruct sparse cardiac DTI data for all directions at the same time with appropriate constraints.

2 Methods

2.1 Constrained Reconstruction

The most common technique to reconstruct cardiac MR DTI data is by applying an inverse 2D Fourier transform on fully acquired k-space data for each image. A separate image is acquired with gradients at different directions to give diffusion weighting at different orientations. At least six images, and a separate reference image without diffusion weighting, are obtained to determine the diffusion tensor and fiber orientations. When full data for each image direction are not acquired in k-space, reconstruction using the inverse Fourier transform leads to aliasing in the images. We have previously shown that the aliasing due to undersampling the data can be resolved using a regularization framework with different constraints [4, 5, 6]. For cardiac DTI, we chose two constraints, one in the dimension of diffusion weighting direction and the other, a spatial constraint. The constraint chosen in the dimension of diffusion direction is the total variation constraint. This constraint was chosen in order to preserve the sharp gradients in the diffusion-weighting direction dimension for each pixel in the image while resolving the artifacts due to undersampling. This constraint is mathematically represented in equation (1) below.

$$T = \sum_{i=1}^{N} \left\| \sqrt{\nabla_d \tilde{m}_i^2 + \beta^2} \right\|_1 \tag{1}$$

In the above equation, N is the total number of pixels in each image direction, ∇_d represents the rate of change in the diffusion weighting direction dimension, $\tilde{m}_i$ is the vector of complex pixel values in the diffusion weighting direction dimension of pixel i in the estimated image space data. β is a small positive constant and $\| \ \|_1$ represents the L1 norm.

The spatial constraint we chose is also a total variation constraint in order to preserve the spatial image gradients. The spatial constraint is shown below in equation (2).

$$S = \sum_{j=1}^{M} \left\| \sqrt{\nabla_x \tilde{m}_j^2 + \nabla_y \tilde{m}_j^2 + \beta^2} \right\|_1 \tag{2}$$

In the above equation, M represents total number of image directions in a given sequence for a single slice, ∇_x is the spatial gradient of the image in the x-direction, ∇_y is the spatial gradient in the y-direction and $\tilde{m}_j$ represents the complex image data for direction j in the given sequence.

Reconstruction from sparse data is performed using the constraints in equations (2) and (3) and preserving fidelity to the acquired sparse data. Reconstruction is performed by minimizing the cost function C given in equation (3) below.

$$\min_{\tilde{m}}(C) = \min_{\tilde{m}} \begin{bmatrix} \left\| WF\tilde{m} - \tilde{d} \right\|_2^2 + \alpha_1 \sum_{i=1}^{N} \left\| \sqrt{\nabla_d \tilde{m}_i^2 + \beta^2} \right\|_1 \\ + \alpha_2 \sum_{j=1}^{M} \left\| \sqrt{\nabla_x \tilde{m}_j^2 + \nabla_y \tilde{m}_j^2 + \beta^2} \right\|_1 \end{bmatrix} \tag{3}$$

In the above equation (3), W represents the binary sparsifying pattern used to obtain sparse k-space data, $\tilde{d}$ which is from the full k-space data and $\| \ \|_2$ represents the L2 norm. α_1 and α_2 are the regularization parameters which are the weighting factors for the constraints. An iterative gradient descent technique with finite forward differences was used to minimize the above function. The complex image data was updated iteratively according to equation (4) shown below.

$$\tilde{m}^{n+1} = \tilde{m}^n - \lambda C'(\tilde{m}^n);\ n = 0,1,2... \tag{4}$$

In the above equation, n represents the iteration number, λ is the step size of the gradient descent method and $C'(\tilde{m})$ is the Euler-Lagrange derivative of the cost function, C in equation (3) with respect to $\tilde{m}$, which is given in equation (5) below.

$$C'(\tilde{m}) = \left\{ \begin{matrix} 2*(F^{-1}(WF\tilde{m}) - F^{-1}(\tilde{d})) - \alpha_1 \nabla_d \left(\frac{\nabla_d \tilde{m}}{\sqrt{\nabla_d \tilde{m}^2 + \beta^2}}\right) \\ -\alpha_2 \begin{pmatrix} \nabla_x \left(\frac{\nabla_x \tilde{m}}{\sqrt{\nabla_x \tilde{m}^2 + \nabla_y \tilde{m}^2 + \beta^2}}\right) \\ + \nabla_y \left(\frac{\nabla_y \tilde{m}}{\sqrt{\nabla_x \tilde{m}^2 + \nabla_y \tilde{m}^2 + \beta^2}}\right) \end{pmatrix} \end{matrix} \right\} \tag{5}$$

2.2 Cardiac DTI Data

To test the above method, retrospective DTI experiments were simulated from datasets acquired in separate studies, including (a) diffusion-weighted spin-echo images (128 x 64 matrix size, 3.0 cm FOV, 2.0 mm thickness) encoded in 6 directions and 8 gradient levels per direction (48 images total) of excised dog heart right ventricular specimens at 7.1 T [2], and (b) diffusion-weighted images (256 x 256 matrix size, 10.0 cm FOV, 3.0 mm thickness) encoded in 12 directions of the left ventricle equatorial slice of intact sheep heart acquired at 2.0 T [3]. Two different undersampling schemes were used to generate sparse data from full k-space data. Fully acquired k-space data for each image direction was sparsified by removing phase encode lines in a variable density fashion in which 8 lines around the center of k-space for each image direction were kept and the phase encodes away from the center were removed in a random fashion. Fig. 1a shows such an undersampling binary mask for a single image direction in the sequence. This sampling scheme was chosen as random undersampling can lead to less severe artifacts as compared to interleaved undersampling. The acceleration factor was defined as the ratio of the number of phase encodes acquired for full data to the number of phase encodes kept for the reconstruction. The second undersampling scheme was radial undersampling in which fully acquired rectilinear k-space data was first sampled on 256 radial lines to simulate radial data. Sparsification was done by removing the radial lines for each image direction. The set of radial spokes for each image direction were rotated by a random angle for different image directions in the sequence. Fig. 1b shows an example of a binary radial mask used to undersample full data in radial fashion. Acceleration factor was defined as the ratio of the number of radial lines in the full data (256) to the number of lines kept for reconstruction.

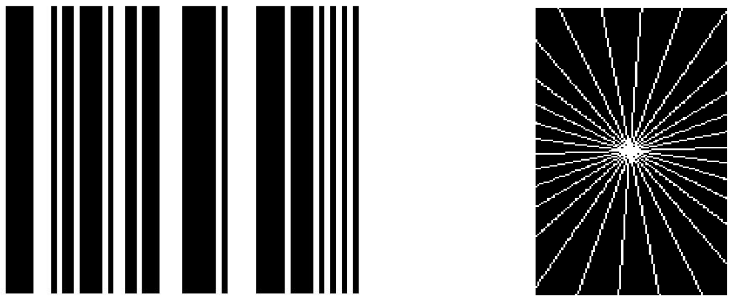

(a) (b)

Fig. 1. (a) Image showing the binary mask for a single image direction to undersample full k-space data in variable density fashion by a factor of two. Six lines around the center of k-space are sampled and the lines outside are sampled in a random fashion. The white portion represents the region of k-space sampled. The phase encoding direction is horizontal. **(b)** Image showing the binary mask for a single image direction to undersample full data in radial fashion. White portion is the region of k-space sampled.

3 Results

3.1 Rectilinear Undersampling – Canine Heart Specimen

The results of the above approach for variable density undersampling by a factor of R=2 are shown in Fig. 2. Fig. 2a shows an image direction for a direction reconstructed from full k-space data using 2D inverse Fourier transform (IFT) with a line passing through it. Fig. 2b shows the corresponding image direction from sparse data using the constrained reconstruction method. Fig. 2c compares the corresponding signal intensity profiles for the images in Fig. 2a and Fig. 2b for the line shown in Fig. 2a.

Three sets of diffusion tensors were computed using (i) reconstructions from full data, (ii) reconstructions from sparse data using constrained approach and (iii) using

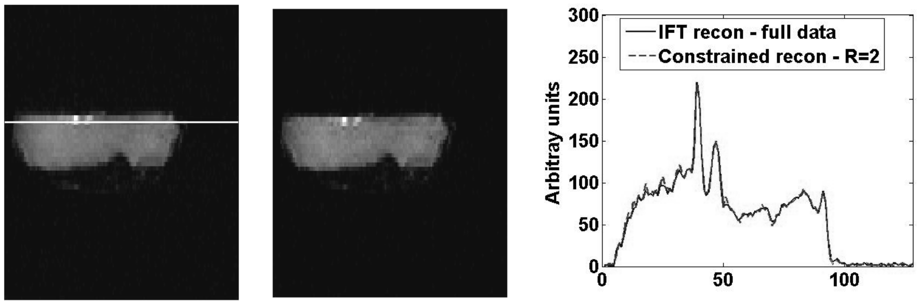

(a) (b) (c)

Fig. 2. **(a)** Image from the canine ex vivo heart specimen showing one diffusion encoded direction reconstructed from full data using IFT. A line passing through the image is also shown. **(b)** Corresponding image reconstructed from sparse data R=2 using the constrained reconstruction approach. **(c)** Comparison of the intensity profiles for the line shown in Fig. 2a for the images in Fig. 2a and Fig. 2b.

only half the number of image directions in the full dataset, for different datasets for different slices. The difference angles between the primary diffusion tensor eigenvectors (fiber orientations) were then computed. Fig. 3 shows the results on a single dataset, which shows the potential of the constrained approach. Fig. 3a shows the difference angle map between full data reconstructions and sparse data reconstructions. Fig. 3b shows the difference angle map between full data and using only half data. The mean deviation angle for the full-sparse is 8.84 ± 0.03 degrees while the value for full-half is 10.44 ± 0.03 degrees. This implies that the sparse data reconstruction using the constrained approach is better at capturing DTI fiber orientation.

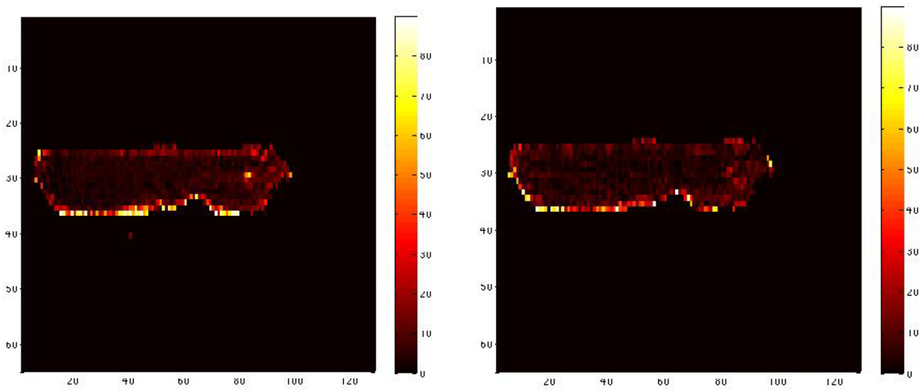

(a) (b)

Fig. 3. **(a)** Difference angle map between full data reconstructions using IFT and sparse data R=2 using the constrained reconstruction method. **(b)** Difference angle map between full data reconstructions using IFT and half the number of image directions reconstructed using IFT.

3.2 Radial Undersampling – Canine Heart Specimen

Results of the constrained reconstruction approach on radially undersampled data are shown in Fig. 4. Fig. 4a shows an image direction for a direction reconstructed from full k-space data with a line passing through it. Fig. 4b shows the corresponding image direction from sparse data, R=4 using the constrained reconstruction method. Fig. 4c compares the corresponding signal intensity profiles for the images in Fig. 4a and Fig. 4b for the line shown in Fig. 4a.

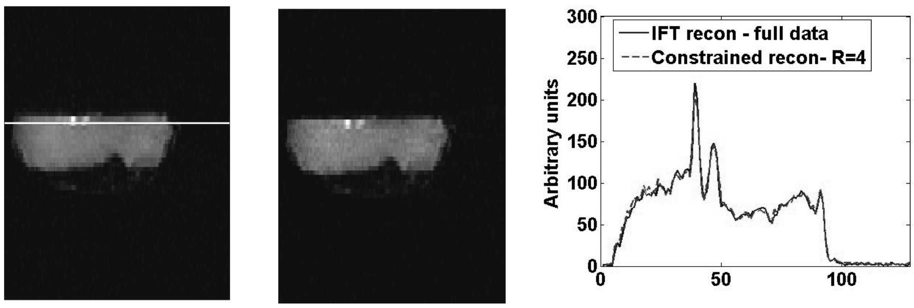

(a) (b) (c)

Fig. 4. (a) Image showing a diffusion weighted direction reconstructed from full k-space data. A line passing through the image is also shown. **(b)** Corresponding image reconstructed from sparse data R=4 using the constrained reconstruction approach. **(c)** Comparison of the intensity profiles for the line shown in Fig. 4a for the images in Fig. 4a and Fig. 4b.

3.3 Rectilinear Undersampling – Sheep Heart

The results of the constrained approach for R=2 data undersampled in variable density fashion for the sheep heart are presented in Fig. 5. Fig. 5a shows a single direction image reconstructed from full k-space data using IFT. Fig. 5b shows the corresponding image reconstructed from sparse data using the current method. The absolute difference image between Fig. 5a and Fig. 5b is shown in Fig. 5c. The peak intensity value in the Fig. 5c was about 15% of the peak intensity value in Fig. 5a.

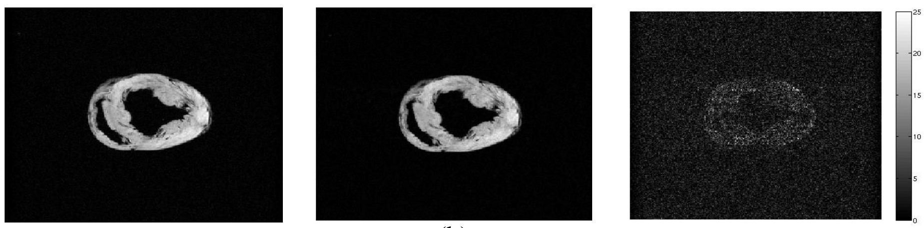

(a) (b) (c)

Fig. 5. (a) Image showing a diffusion weighted direction reconstructed from full k-space data for the sheep heart. **(b)** Corresponding image reconstructed from sparse data R=2 using the constrained reconstruction approach. **(c)** Absolute difference image between Fig. 5a and Fig. 5b.

4 Discussion

The parameters in the reconstruction method were empirically chosen based on the results for different datasets. The method was robust to small variation in the regularization parameters. We also note that formal methods, like the L-surface [7] technique can be used to determine the regularization parameters.

We found that the spatial and temporal constraints were almost equally helpful in reducing the artifacts from undersampling. Fig. 6 compares the effects of spatial and temporal constraints. Fig. 6a shows the absolute difference image between full data reconstruction using IFT and image reconstructed using IFT from R=2 data for a single image direction. Fig. 6b shows the absolute difference image between full data reconstruction using IFT and image reconstructed using only the temporal constraint, that is α_1 set to the empirical value and α_2 is set to zero in equation (3). Fig. 6c shows the absolute difference image between the image reconstructed from full data using IFT and the image reconstructed from R=2 data using spatial constraint only

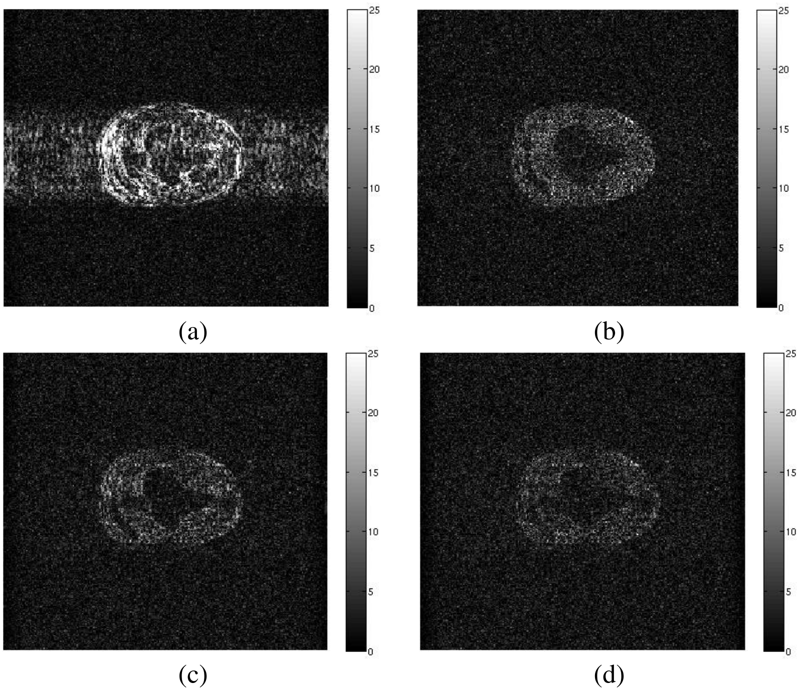

Fig. 6. (a) Image showing the absolute difference between full data reconstruction using IFT and R=2 data using IFT for a single image direction. **(b)** Image showing the absolute difference between full data reconstruction using IFT and R=2 data using only the temporal constraint. **(c)** Corresponding absolute difference image between full data reconstruction using IFT and R=2 data using spatial constraint only. **(d)** Corresponding absolute difference image between full data reconstruction using IFT and R=2 data using both spatial and temporal constraints.

that is α_1 is set to zero and α_2 is set to the empirical value in equation (3). Fig 6d shows the corresponding absolute difference between image reconstructed using full data using IFT and the image reconstructed using both spatial and temporal constraints. We can see that both the spatial and temporal constraints independently help reduce the artifacts but when combined together perform better in reducing the artifacts due to undersampling.

It is expected that the joint constrained reconstruction approach will perform better when more diffusion-weighted directions are measured. This is because neighboring directions are not independent, but have correlations. These correlations are implicitly used in the reconstruction to give "lossless" reconstructions from less data. Early results show the 12 direction sheep heart dataset performed better qualitatively than the 6 direction canine heart specimen dataset. Further work is needed to quantify these differences.

A limitation of the current study is that the results are from post-acquisition downsampling. Actually changing the DTI acquisition to acquire fewer phase encodes would be advantageous in terms of image artifacts, but could lead to either better or worse performance of the reconstruction method.

It was found that radial undersampling provided higher accelerations using the reconstruction method as compared to rectilinear undersampling. This could be due to the fact that radial undersampling leads to less severe artifacts as compared to rectilinear undersampling. Note that another limitation of the study is that the radial k-space data was generated from rectilinear k-space measurements, so do not reflect the actual measurements that would be made with a radial pulse sequence.

5 Conclusions

A constrained approach to reconstruct sparse cardiac DTI was proposed. The method has the potential to improve cardiac diffusion tensor imaging by acquiring less data in each diffusion weighted direction while reconstructing the entire set of diffusion-weighted images from multiple directions simultaneously. The method was tested on k-space data undersampled in both rectilinear and radial patterns. The results showed that the diffusion-weighted images could be reconstructed with little loss in the image quality.

References

[1] Hsu, E., Muzikant, A.L., Matulevicius, S.A., Penland, R.C., Henriquez, C.: Magnetic resonance myocardial fiber-orientation mapping with direct histological correlation. Am J Physiol, 274(5 Pt 2), H1627–1634 (1998)

[2] Hsu, E., Henriquez, C.: Myocardial fiber orientation mapping using reduced encoding diffusion tensor imaging. J. Cardiovasc. Magn. Reson. 3, 339–347 (2001)

[3] Jiang, Y., Hsu, E.: Accelerating MR diffusion tensor imaging via filtered reduced-encoding projection-reconstruction. Magn. Reson. Med. 53, 93–102 (2005)

[4] Adluru, G., Whitaker, R.T., DiBella, E.V.R.: Spatio-Temporal Constrained Reconstruction of sparse dynamic contrast enhanced radial MRI data. In: Proc. IEEE ISBI (To appear) (2007)

[5] Adluru, G., Awate, S.P., Tasdizen, T., Whitaker, R.T., DiBella, E.V.R.: Temporally Constrained Reconstruction of dynamic cardiac perfusion MRI. Magn. Reson. Med. (To appear) (2007)

[6] Portniaguine, O., Bonifasi, C., DiBella, E.V.R., Whitaker, R.T.: Inverse methods for reduced k-space acquisition. In: Proceedings of the ISMRM 11th Annual Meeting, Toronto, p. 481 (2003)

[7] Belge, M., Kilmer, M.E., Miller, E.L.: Efficient determination of Multiple Regularization Parameters in a Generalized L-curve Framework. Inverse Problems 18, 1161–1183 (2002)